PHYSICAL REVIEW B VOLUME 2, NUMBER 7 1 OCTOBER 1970

Inelastic Neutron Scattering from Itinerant Electron Antiferromagnets: Theory*

S. H. Liu
Institute for Atomic Research and Department of Physics, Iowa State University, Ames, Iowa 50010
(Received 11 May 1970)

Inelastic neutron scattering cross section for a simple model of itinerant electron antiferromagnets is calculated in both the ordered and the disordered temperature regions. The depairing effect due to impurity and phonon scattering is taken into account in terms of a phenomenological electron level width. It is found that at low temperatures, where the electron lifetime is long, the neutrons interact with spin waves as described by earlier theories. As the temperature is raised, the spin-wave lines broaden continuously with very slight change of velocity. Near, but below the Néel temperature, the energy gap vanishes, and the spin-wave lines become ill-defined peaks having a flat top centered at the magnetic reciprocal-lattice point. Finally, above the Néel temperature, the excitations are the well-known paramagnons. The Stoner type of mode is found to be extremely broadened even at low temperatures ($T \cong 0.5T_N$), so that they are not observable by means of neutrons. The electron mass enhancement due to magnon and paramagnon interactions is also discussed.

I. INTRODUCTION

Chromium and some chromium-rich alloys are found to be antiferromagnetically ordered at low enough temperatures but possess no localized magnetic moment above the ordering temperature.[1-7] These are classified as itinerant electron antiferromagnets because the magnetic ordering comes about as a condensed quantum state of the conduction electrons (spin-density-wave state) very similar to the superconducting state in metals.[8-17] Consequently, one expects the collective excitations in these metals to be quite different in nature from the spin waves in Heisenberg-type antiferromagnets. The most powerful method to use in studying these excitations is the inelastic neutron scattering technique, and experimental results for CrMn alloys have been reported by Als-Nielsen and Dietrich[18] and by Sinha *et al.*[19] In this paper we follow up Ref. 19 and report the details of our theoretical study on this subject.

The fact that the ordered state of chromium is a static spin-density wave of the conduction electrons was first recognized by Overhauser.[8,9] Lomer[10] pointed out that the spin-density-wave state should be energetically more stable than the paramagnetic state because the Fermi-surface structure of chromium allows different pieces of flat surfaces to nest into each other. A mathematical model utilizing the nesting of Fermi surfaces was worked out by Fedders and Martin.[11] In this model one assumes two parabolic bands, one for electrons and one for holes. The Fermi surfaces of these bands are identical spheres which nest into each other at every point. As a result of the exchange interaction between the electrons, the electrons of one band move coherently with the holes in the other band and form a condensed state with long-range order. An energy gap develops at the Fermi level, and the thermodynamic and magnetic properties of the system are expressible in terms of the energy gap. Thus, the gap may be regarded as an order parameter. A number of subsequent papers deal with more realistic energy-band and Fermi-surface models.[12-16] Zittartz[17] showed that the coherent motion of the electron-hole pair can be broken up by scattering with phonons or impurities. In fact, when the scattering is sufficiently strong, the energy gap may disappear even though the system is still in the ordered state. Therefore, a realistic theory must distinguish between the energy gap and the order parameter, a situation analogous to the theory of gapless superconductivity.[20,21]

The collective excitations of the spin-density-wave state have been discussed by Fedders and Martin[11] on the basis of a two-band model and by Sokoloff[16] in terms of the Hubbard model. The purpose of this work is to carry out the spin-wave calculation at finite temperatures and to include the scattering effects. We use the diagrammatic technique to evaluate a double-time nonlocal susceptibility function for the electron gas and then relate this function to the neutron cross section. The method is very similar to that for calculating the transport coefficients of superconductors,[20-27] except that we must generalize the calculation to include the wave-vector dependence. One should be able to use this method to calculate the nonlocal response functions for superconductors as well.

II. MODEL

We choose to work with a one-dimensional energy-band model as shown in Fig. 1. We assume that there are two straight bands for electrons and holes and that the band energy depends only on the z component of the wave vector, i.e.,

$$E_{1\vec{k}} = v|k_z|$$

for electrons, and

$$E_{2\vec{k}} = 2\mu - v|k_z - \tfrac{1}{2}g| \qquad (2.1)$$

for holes, where μ is the Fermi energy and g is the length of the reciprocal-lattice vector $\vec{g}$ in the z direction. The bands are cut off somewhere in the x, y directions. The entire band structure repeats itself in the z direction with the periodicity g, and the wave vector of the spin-density wave is $\frac{1}{2}\vec{g}$. Although this model is very simple, it is rather close to reality because the nesting portions of the Fermi surface in chromium are very flat and the separation between the surfaces is nearly one-half the reciprocal-lattice vector. Adding a few percent of manganese makes the magnetic structure commensurate with the lattice structure, and the magnetic periodicity is exactly as described by our model.

The Hamiltonian of the system is taken as

$$H = H_0 + H_1 + H_2 ,$$

where

$$H_0 = \sum_{\vec{k}s} (E_{1\vec{k}} c^\dagger_{1\vec{k}s} c_{1\vec{k}s} + E_{2\vec{k}} c^\dagger_{2\vec{k}s} c_{2\vec{k}s}) \quad ,$$

which is the band energy of the electrons,

$$H_1 = \tfrac{1}{2} V \sum_{\vec{k}\vec{k}'\vec{q}s} c^\dagger_{1\vec{k}s} c_{1,\vec{k}-\vec{q},s} c^\dagger_{2\vec{k}',-s} c_{2,\vec{k}'+\vec{q},-s} \quad ,$$

which is the exchange energy between the electrons, and

$$H_2 = u \sum_i \sum_{n\vec{k}\vec{k}'s} c^\dagger_{n\vec{k}s} c_{n\vec{k}'s} e^{i(\vec{k}'-\vec{k})\cdot\vec{R}_i} \quad , \qquad (2.2)$$

which is the scattering interaction. The exchange interaction is truncated to allow only the terms

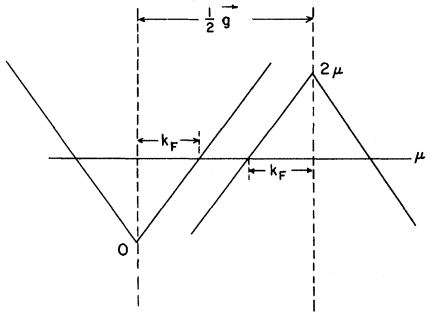

FIG. 1. One-dimensional band model for the susceptibility calculations.

which are relevant to the antiferromagnetic coupling, i.e., the repulsive interaction between electrons with opposite spins in different bands. The scattering is from a random set of fixed impurities, although, in the end, the scattering lifetime will be treated as a temperature-dependent quantity in order to include also the phonon scattering. The assumption of elastic scattering makes it possible to sum up certain diagrams in a straightforward manner.

We define a two-component spinor operator

$$\psi_{\vec{k}s} = \begin{pmatrix} c_{1\vec{k}s} \\ c_{2,\vec{k}+(1/2)\vec{g},-s} \end{pmatrix} \quad , \qquad (2.3)$$

and a 2×2 Green's function

$$\vec{G}_{\vec{k}s}(\tau s) = \langle T\psi_{\vec{k}s}(\tau)\psi^\dagger_{\vec{k}s}(0)\rangle \quad , \qquad (2.4)$$

where

$$\psi_{\vec{k}s}(\tau) = e^{-\tau(\mu N - H)}\psi_{\vec{k}s}e^{\tau(\mu N - H)} \quad ,$$
$$N = \sum_{n\vec{k}s} c^\dagger_{n\vec{k}s} c_{n\vec{k}s} \quad , \qquad (2.5)$$

which is the number of particle operator, τ is the imaginary time, and T is the imaginary time-ordering operator. The symmetry between up and down spin implies that $\vec{G}_{\vec{k}s}(\tau)$ is independent of the spin. The Fourier transform of $\vec{G}_{\vec{k}}(\tau)$ is defined by

$$\vec{G}_{\vec{k}}(\tau) = (1/\beta)\sum_l \vec{G}(\vec{k}, \nu_l) e^{-i\nu_l\tau} , \qquad (2.6)$$

where $\nu_l = (2l+1)\pi/\beta$, $\beta = 1/k_B T$, and l is an integer. In the absence of scattering we can write down the zeroth-order Green's function

$$[\vec{G}^{(0)}(\vec{k}, \nu_l)]^{-1} = \begin{pmatrix} \epsilon_{\vec{k}} - i\nu_l & \Delta \\ \Delta & -\epsilon_{\vec{k}} - i\nu_l \end{pmatrix}, \qquad (2.7)$$

where

$$\epsilon_{\vec{k}} = E_{1\vec{k}} - \mu = v(|k_z| - k_F) \quad , \qquad (2.8)$$

and k_F is the Fermi wave vector defined by $vk_F = \mu$. A self-energy correction due to the exchange interaction is ignored because this term should be regarded as a part of the band energy. The energy gap 2Δ is given by

$$\Delta = V\sum_{\vec{k}} \langle c_{1\vec{k}s} c^\dagger_{2,\vec{k}+(1/2)\vec{g},-s}\rangle \quad . \qquad (2.9)$$

The expectation values on the right-hand side of Eq. (2.9) may be related to the off-diagonal elements of the Green's function. One then obtains an integral equation for Δ, and this reproduces the Fedders-Martin theory.

When the scattering interaction is included, we find in general, with a proper choice of the phase of Δ,

$$\vec{G}(\vec{k}, \nu_l) = \begin{pmatrix} G(\vec{k}, \nu_l) & F(\vec{k}, \nu_l) \\ F(\vec{k}, \nu_l) & -G(\vec{k}, -\nu_l) \end{pmatrix} , \quad (2.10)$$

where the relationship between $\vec{G}$ and $\vec{G}^{(0)}$ is

$$\vec{G}^{-1} = (G^{(0)})^{-1} - \vec{\Sigma} , \quad (2.11)$$

and $\vec{\Sigma}$ is the self-energy due to scattering. Following the work of Abrikosov and Gor'kov[20] and Zittartz[17] we write the self-energy as

$$\vec{\Sigma}(\vec{k}, \nu_l) = n_i |u|^2 \sum_{\vec{k}'} \vec{G}(\vec{k}', \nu_l) , \quad (2.12)$$

where n_i is the density of scatterers. Then, the matrix $\vec{\Sigma}$ has the form

$$\vec{\Sigma}(\vec{k}, \nu_l) = \begin{pmatrix} \Sigma_1(\vec{k}, \nu_l) & \Sigma_2(\vec{k}, \nu_l) \\ \Sigma_2(\vec{k}, \nu_l) & -\Sigma_1(\vec{k}, -\nu_l) \end{pmatrix} . \quad (2.13)$$

If we define two new functions Z and $\bar{\Delta}$,

$$\begin{aligned} \Sigma_1(\vec{k}, \nu_l) &= i\nu_l [Z(\nu_l) - 1] , \\ \Sigma_2(\vec{k}, \nu_l) &= \Delta - \bar{\Delta}(\nu_l) Z(\nu_l) , \end{aligned} \quad (2.14)$$

then we can solve Eq. (2.12) and find

$$\begin{aligned} Z(\nu_l) &= 1 + \Gamma/2E_l , \\ \bar{\Delta}(\nu_l) &= \Delta[1 + \Gamma/E_l] , \end{aligned} \quad (2.15)$$

$$G(\vec{k}, \nu_l) = \frac{1}{Z(\nu_l)} \frac{\bar{\epsilon}_{\vec{k}} + i\nu_l}{\nu_l^2 + \bar{\epsilon}_{\vec{k}}^2 + \bar{\Delta}^2(\nu_l)} ,$$

$$F(\vec{k}, \nu_l) = \frac{1}{Z(\nu_l)} \frac{\bar{\Delta}(\nu_l)}{\nu_l^2 + \bar{\epsilon}_{\vec{k}}^2 + \bar{\Delta}^2(\nu_l)} ,$$

where

$$\begin{aligned} \bar{\epsilon}_{\vec{k}} &= \epsilon_{\vec{k}}/Z(\nu_l) , \\ E_l &= [\nu_l^2 + \bar{\Delta}^2(\nu_l)]^{1/2} , \\ \Gamma &= 2\pi n_i |u|^2 N(0) , \end{aligned} \quad (2.16)$$

n_i is the density of scatterers, and $N(0)$ is the density of states for one band and one spin at the Fermi level. The value of $N(0)$ depends on the cutoff wave vectors of the energy bands, in x, y directions. However, there is no need to specify these cutoff wave vectors because we will use $N(0)$ as a parameter in the theory. The quantity Γ is the width of the electron level. The self-consistent equation for the order parameter has the form

$$\Delta = N(0) V (\pi/\beta) \sum_l [\bar{\Delta}(\nu_l)/E_l] ,$$

or equivalently

$$1 = N(0) V (\pi/\beta) \sum_l 1/(E_l + \Gamma) . \quad (2.17)$$

To solve this equation one must analytically continue the equation into the real frequency domain and solve the resulting integral equation numerically as done in Ref. 21. If we set $\nu_l = -i\omega + 0^+$ and define

$$\bar{\Delta}(-i\omega + 0^+) = \Delta_1(\omega) + i\Delta_2(\omega) ,$$

then $2\Delta_1(0)$ is the energy gap of the system. The condition for gaplessness is $\Gamma \geq \Delta$.

In our numerical analysis, we choose Γ as a function of the temperature

$$\Gamma = \Gamma_0 + \alpha T , \quad (2.18)$$

where $\Gamma_0 = 7.8$ meV is the line broadening due to impurity scattering as estimated from the residual resistivity and $\alpha = 0.13$ meV/K is the temperature coefficient for the phonon scattering broadening as estimated from the McMillan formula.[28] This formula for Γ should be reliable for high temperatures, but is not valid below the Debye temperature, where $\Gamma(T)$ should obey a higher power law. In this study we are interested only in the behavior of the material at room temperature and above. The quantity $N(0)V = 0.43$ is chosen to fit the observed Néel temperature of 515 K for an alloy containing 2% Mn, and the Fermi level μ is taken as 1 eV. The results of solving the gap equation are plotted in Fig. 2, where the order parameter Δ, the half-gap $\Delta_1(0)$, and the electron level width Γ are shown as functions of the temperature. The magnetic moment per ion is proportional to the order parameter. The linear drop of Δ at low temperatures results from the assumed linear temperature dependence of Γ. If we use a higher power law for Γ we would get a more gradual drop of the order parameter with increasing temperature. The

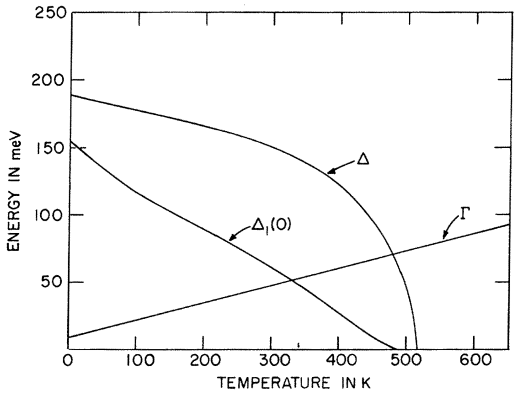

FIG. 2. Order parameter, energy gap, and electron linewidth for the model of CrMn alloy.

energy gap at low temperatures is calculated to be 310 meV compared with the measured value of 370 meV for a comparable alloy.[29] The discrepancy may be partly due to the crude assumption of $\Gamma(T)$ and partly due to the band model, because imperfect nesting of the real Fermi surfaces always increases the ratio $2\Delta_1(0)/k_B T_N$.[14] The energy gap disappears at about 35 K below the Néel temperature.

III. CALCULATION OF THE SUSCEPTIBILITY FUNCTION

The differential scattering cross section of neutrons by a magnetic system is of the form[30,31]

$$\left(\frac{d^2\sigma}{d\Omega d\omega}\right)_{\text{mag}} \propto \sum_{\alpha\beta} (\delta_{\alpha\beta} - \hat{q}_\alpha \hat{q}_\beta) \frac{\text{Im}\chi_{\alpha\beta}(\vec{q}, \omega)}{1 - e^{-\beta\omega}} , \quad (3.1)$$

where $\vec{q}$ and ω are, respectively, the momentum and energy transfer from the neutron to the electron gas ($\hbar = 1$), $\beta = 1/k_B T$, and we have omitted factors which are slowly varying in the neighborhood of the magnetic reciprocal-lattice point. For an electron gas the susceptibility function $\chi_{\alpha\beta}(\vec{q}, \omega)$ has the form[22,31]

$$\chi_{\alpha\beta}(\vec{q}, \omega) = \chi_{\alpha\beta}(\vec{q}, \omega_n)\big|_{\omega_n = -i\omega + 0^+} ,$$

$$\chi_{\alpha\beta}(\vec{q}, \omega_n) = \tfrac{1}{4} \sum_{\vec{k}s} \sum_{\vec{k}'s'} \int_0^\beta \langle T\psi^\dagger_{\vec{k}+\vec{q},s}(\tau)\sigma^\beta \times \psi_{\vec{k}s}(\tau)\psi^\dagger_{\vec{k}'s'}(0)\sigma^\alpha \psi_{\vec{k}'+\vec{q},s'}(0)\rangle e^{i\omega_n \tau} d\tau , \quad (3.2)$$

where σ^α ($\alpha = 1, 2, 3$) are Pauli spin matrices, $\omega_n = 2\pi n/\beta$, and n is an integer.

In the Hartree-Fock approximation, we contract the electron operators in pairs and obtain

$$\chi^{HF}_{\alpha\beta}(\vec{q}, \omega_n) = -\frac{1}{4\beta} \sum_{ijpr} \sum_{\vec{k}l} \sigma^\beta_{ij} G_{jp}(\vec{k}, \nu_l) \times \sigma^\alpha_{pr} G_{ri}(\vec{k}+\vec{q}, \nu_l + \omega_n), \quad (3.3)$$

where G_{ij} are components of the matrix $\tilde{G}$. Because of the exchange and scattering interactions, we must make two sets of corrections to this result.

Consider first the scattering from impurities. By examining the structure of the Hartree-Fock term, we may infer that, after the scattering correction is made, we should get

$$\chi^{(0)}_{\alpha\beta}(\vec{q}, \omega_n) = -\frac{1}{4\beta} \sum_{ijpr} \sum_{l} \sigma^\beta_{ij} \tilde{\alpha}_{ji,pr} \sigma^\alpha_{pr} . \quad (3.4)$$

Then the matrix $\tilde{\alpha}$ must satisfy the equation

$$\alpha_{ji,pr}(\vec{q}, \omega_n, \nu_l) = \mathcal{B}_{ji,pr}(\vec{q}, \omega_n, \nu_l) + n_j |u|^2 \times \sum_{st} \mathcal{B}_{ji,st}(\vec{q}, \omega_n, \nu_l) \alpha_{st,pr}(\vec{q}, \omega_n, \nu_l) , \quad (3.5)$$

where

$$\mathcal{B}_{ji,pr}(\vec{q}, \omega_n, \nu_l) = \sum_{\vec{k}} G_{jp}(\vec{k}, \nu_l) G_{ri}(\vec{k}+\vec{q}, \nu_l + \omega_n) . \quad (3.6)$$

Equation (3.5) is diagrammatically represented in Fig. 3. The matrix $\tilde{\alpha}$ is solved by a simple inversion.

It can be verified that, after considering the translational and spin symmetries,

$$\tilde{\mathcal{B}} = \begin{pmatrix} a_l & b_l & c_l & d_l \\ b_l & a_l & d_l & c_l \\ c_l & d_l & a_l & b_l \\ d_l & c_l & b_l & a_l \end{pmatrix} , \quad (3.7)$$

where the rows and columns of the matrix are labeled by the pairs of indices 11, 22, 12, 21, and the matrix elements

$$\begin{aligned} a_l &= \sum_{\vec{k}} G(\vec{k}, \nu_l) G(\vec{k}+\vec{q}, \nu_l + \omega_n) , \\ b_l &= \sum_{\vec{k}} F(\vec{k}, \nu_l) F(\vec{k}+\vec{q}, \nu_l + \omega_n) , \\ c_l &= \sum_{\vec{k}} G(\vec{k}, \nu_l) F(\vec{k}+\vec{q}, \nu_l + \omega_n) , \\ d_l &= \sum_{\vec{k}} F(\vec{k}, \nu_l) G(\vec{k}+\vec{q}, \nu_l + \omega_n) . \end{aligned} \quad (3.8)$$

The matrix $\tilde{\alpha}$ is found to be

$$\tilde{\alpha} = \begin{pmatrix} \rho_l & \xi_l & \eta_l & \zeta_l \\ \xi_l & \rho_l & \zeta_l & \eta_l \\ \eta_l & \zeta_l & \rho_l & \xi_l \\ \zeta_l & \eta_l & \xi_l & \rho_l \end{pmatrix} , \quad (3.9)$$

where

$$\rho_l \pm \xi_l \pm \eta_l \pm \zeta_l = \frac{a_l \pm b_l \pm c_l \pm d_l}{1 - n_i |u|^2 (a_l \pm b_l \pm c_l \pm d_l)} . \quad (3.10)$$

There must be an even number of minus signs in Eq. (3.10).

Now we consider the exchange interaction whose basic diagram is shown in Fig. 4. We want to emphasize that only electrons with opposite spins are coupled by the interaction. Hence, of all the possible terms of $\chi^{(0)}_{\alpha\beta}$, only those involving a spin flip are enhanced. These terms are

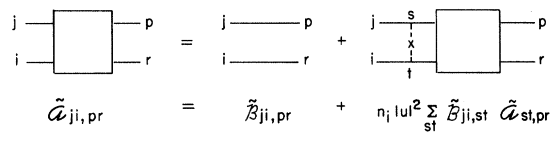

FIG. 3. Diagrams for scattering correction to the unenhanced susceptibility function.

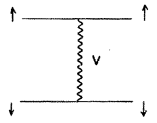

FIG. 4. Basic diagram for exchange interaction.

$$\chi_{+-}^{(0)}(\vec{q},\omega_n)=\chi_{-+}^{(0)}(\vec{q},\omega_n)=-(1/\beta)\textstyle\sum_l \rho_l \quad . \tag{3.11}$$

The ladder diagrams for χ_{+-} are shown in Fig. 5. We denote

$$\chi_1(\vec{q},\omega_n)=\chi_{+-}(\vec{q},\omega_n)=\sum_{\vec{k}\vec{k}'}\int_0^\beta \langle T c^\dagger_{\vec{k}+\vec{q},\downarrow}(\tau)c_{\vec{k}\uparrow}(\tau) \times c^\dagger_{\vec{k}'\uparrow}(0)c_{\vec{k}'+\vec{q},\downarrow}(0)\rangle e^{i\omega_n\tau}d\tau \quad ,$$

$$\chi_2(q,\omega_n)=\sum_{\vec{k}\vec{k}'}\int_0^\beta \langle T c^\dagger_{\vec{k}+\vec{q},\downarrow}(\tau)c_{\vec{k}\uparrow}(\tau) \times c^\dagger_{k'\downarrow}(0)c_{k'+q,\uparrow}(0)\rangle e^{i\omega_n\tau}d\tau \quad . \tag{3.12}$$

Without the exchange interaction, we find

$$\chi_1^{(0)}(\vec{q},\omega_n)=-(1/\beta)\textstyle\sum_l \rho_l \quad ,$$
$$\chi_2^{(0)}(\vec{q},\omega_n)=-(1/\beta)\textstyle\sum_l \xi_l \quad . \tag{3.13}$$

Then we can sum the diagrams in Fig. 5 by solving the equations

$$\chi_1=\chi_1^{(0)}+\chi_1^{(0)}V\chi_1+\chi_2^{(0)}V\chi_2 \quad ,$$
$$\chi_2=\chi_2^{(0)}+\chi_2^{(0)}V\chi_1+\chi_1^{(0)}V\chi_2 \quad . \tag{3.14}$$

From these we find

$$\chi_1=\frac{1}{2}\left(\frac{\chi_1^{(0)}+\chi_2^{(0)}}{1-V(\chi_1^{(0)}+\chi_2^{(0)})}+\frac{\chi_1^{(0)}-\chi_2^{(0)}}{1-V(\chi_1^{(0)}-\chi_2^{(0)})}\right) \quad , \tag{3.15}$$

where

$$\chi_1^{(0)}\pm\chi_2^{(0)}=-\frac{1}{2\beta}\sum_l\left(\frac{a_l\pm b_l+c_l\pm d_l}{1-n_i|u|^2(a_l\pm b_l+c_l\pm d_l)}+\frac{a_l\pm b_l-c_l\mp d_l}{1-n_i|u|^2(a_l\pm b_l-c_l\mp d_l)}\right) \quad . \tag{3.16}$$

Thus, the susceptibility function that is needed for computing the neutron cross section is completely determined.

As mentioned earlier, the susceptibility function χ_{zz} is not enhanced in our calculation. This apparent violation of rotational symmetry arises from the assumed form of H_1. If we assume a rotationally invariant exchange of the form $\vec{s}\cdot\vec{s}$, we would have to enhance the zz component of the susceptibility by summing a set of bubble diagrams.

We now return to Eq. (3.8) and evaluate the sums over $\vec{k}$. To excite spin waves the neutron wave vector $\vec{q}$ must be close to the magnetic wave vector $\frac{1}{2}\vec{g}$. We define $\vec{Q}=\vec{q}-\frac{1}{2}\vec{g}$ and denote the z component of $\vec{Q}$ simply by Q. The condition $|Q|\ll k_F$ is valid in the actual experiment; so, if $\vec{k}$ is in the electron band, $\vec{k}+\vec{q}$ must be in the hole band and vice versa. Hence, in the expression for a_l, we may put $\epsilon_{\vec{k}}=v|k_z|-\mu$ and $\epsilon_{\vec{k}+\vec{q}}=\mu-v|k_z+Q|$ in the Green's functions. For $k_z>0$, we have $\epsilon_{\vec{k}}=vk_z-\mu$, $\epsilon_{\vec{k}+\vec{q}}=-\epsilon_{\vec{k}}-vQ$. Then, the contribution to a_l is

$$\tfrac{1}{2}N(0)\int_{-\mu}^{\mu}d\epsilon_{\vec{k}}G(\vec{k},\nu_l)G(\vec{k}+\vec{q},\nu_l+\omega_n) \quad .$$

We replace the limits by $\pm\infty$ and close the contour above the real axis. The integration over $\epsilon_{\vec{k}}$ yields

$$-\frac{\pi}{4}N(0)\left[\left(1+\frac{\nu_l}{E_l}\right)\left(1+\frac{\nu_{l'}}{E_{l'}}\right)\frac{1}{-ivQ+E_l+E_{l'}+\Gamma}+\left(1-\frac{\nu_l}{E_l}\right)\left(1-\frac{\nu_{l'}}{E_{l'}}\right)\frac{1}{ivQ+E_l+E_{l'}+\Gamma}\right] \quad ,$$

where $\nu_{l'}=\nu_l+\omega_n$ and $E_{l'}=[\nu_{l'}^2+\overline{\Delta}^2(\nu_{l'})]^{1/2}$. For the part $k_z<0$, we have $\epsilon_{\vec{k}}=-vk_z-\mu$, $\epsilon_{\vec{k}+\vec{q}}=-\epsilon_{\vec{k}}+vQ$. The contribution to a_l is given by a similar expression except for a change of sign of Q. Therefore,

$$a_l=-\tfrac{1}{2}\pi N(0)(1+\nu_l\nu_{l'}/E_lE_{l'})F(Q,\nu_l,\omega_n) \quad , \tag{3.17}$$

where

$$F(Q,\nu_l,\omega_n)=1/(ivQ+E_l+E_{l'}+\Gamma)+\text{c.c.} \tag{3.18}$$

In a similar manner we find

$$b_l=\tfrac{1}{2}\pi N(0)[\overline{\Delta}(\nu_l)\overline{\Delta}(\nu_{l'})/E_lE_{l'}]F(Q,\nu_l,\omega_n) \quad ,$$
$$c_l=i\tfrac{1}{2}\pi N(0)[\nu_l\overline{\Delta}(\nu_{l'})/E_lE_{l'}]F(Q,\nu_l,\omega_n) \quad ,$$
$$d_l=i\tfrac{1}{2}\pi N(0)[\overline{\Delta}(\nu_l)\nu_{l'}/E_lE_{l'}]F(Q,\nu_l,\omega_n) \quad . \tag{3.19}$$

In the next step we convert all the quantities in Eq. (3.15) into the real frequency domain. As shown by Ambegaokar and Tewordt[23] the unenhanced susceptibilities have the spectral representations

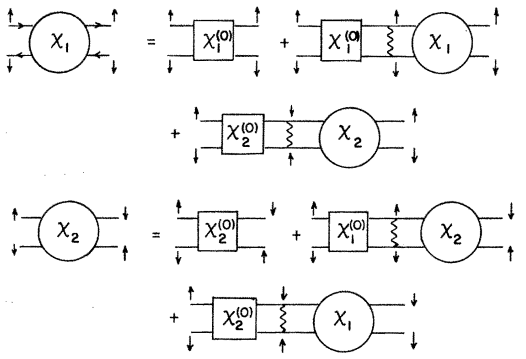

FIG. 5. Diagrams for exchange enhancement calculation.

$$\chi_1^{(0)}(\vec{q}, \omega_n) \pm \chi_2^{(0)}(\vec{q}, \omega_n) = \frac{1}{\beta} \sum_l \int \frac{d\omega_1}{2\pi} \int \frac{d\omega_2}{2\pi} \left(\frac{A_\pm(\omega_1, \omega_2)}{(\omega_1 - i\nu_l)(\omega_2 - i\nu_l - i\omega_n)} + \frac{B_\pm(\omega_1, \omega_2)}{(\omega_1 - i\nu_l)(\omega_1 - \omega_2 + i\omega_n)} \right). \quad (3.20)$$

We write Eq. (3.16) in a condensed form as

$$\chi_1^{(0)}(q, \omega_n) \pm \chi_2^{(0)}(q, \omega_n) = -(1/\beta) \sum_l P_\pm(\nu_l, \nu_l + \omega_n) , \quad (3.21)$$

then the spectral densities $A_\pm$ and $B_\pm$ are related to $P_\pm$ by

$$\begin{aligned} -A_\pm(\omega_1, \omega_2) = {} & P_\pm(-i\omega_1 + 0^+, -i\omega_2 + 0^+) - P_\pm(-i\omega_1 + 0^+, \\ & -i\omega_2 + 0^-) - P_\pm(-i\omega_1 + 0^-, -i\omega_2 + 0^+) \\ & + P_\pm(-i\omega_1 + 0^-, -i\omega_2 + 0^-), \\ B_\pm(\omega_1, \omega_2) = {} & 0. \end{aligned} \quad (3.22)$$

It follows after summing over l that

$$\chi_1^{(0)} \pm \chi_2^{(0)} = \int \frac{d\omega_1}{2\pi} \int \frac{d\omega_2}{2\pi} A_\pm(\omega_1, \omega_2) \frac{f(\omega_2) - f(\omega_1)}{\omega_1 - \omega_2 + i\omega_n},$$

where $f(\omega)$ is the Fermi distribution function. Now we put in $i\omega_n = \omega + i0^+$ and find the imaginary parts of the unenhanced susceptibility functions to be

$$\begin{aligned} I_\pm(\vec{q}, \omega) &= \mathrm{Im}[\chi_1^{(0)}(\vec{q}, \omega) \pm \chi_2^{(0)}(\vec{q}, \omega)] \\ &= \frac{1}{2} \int \frac{d\omega_1}{2\pi} A_\pm(\omega_1, \omega_2)[f(\omega) - f(\omega_1 + \omega)] . \end{aligned} \quad (3.23)$$

The real parts may be obtained from the dispersion relation

$$\begin{aligned} R_\pm(\vec{q}, \omega) &= \mathrm{Re}[\chi_1^{(0)}(\vec{q}, \omega) \pm \chi_2^{(0)}(\vec{q}, \omega)] \\ &= \frac{1}{\pi} \int_{-\infty}^{\infty} \frac{I_\pm(\vec{q}, \omega')}{\omega' - \omega} \, d\omega' . \end{aligned}$$

The above integral can be made to converge much faster by making a subtraction

$$R_\pm(\vec{q}, \omega) = R_\pm(\vec{q}, 0) - \frac{2\omega^2}{\pi} \int_0^{\infty} \frac{I_\pm(\vec{q}, \omega')}{\omega'(\omega'^2 - \omega^2)} \, d\omega' , \quad (3.24)$$

where

$$R_\pm(\vec{q}, 0) = -(1/\beta) \sum_l P_\pm(\nu_l, \nu_l) . \quad (3.25)$$

When the sum is converted to an integral, we find

$$\begin{aligned} R_\pm(\vec{q}, 0) = {} & (i/2\pi) \int_{-\infty}^{\infty} [P_\pm(-i\omega + 0^+, -i\omega + 0^+) \\ & - P_\pm(-i\omega + 0^-, -i\omega + 0^-)] \tanh \tfrac{1}{2}\beta\omega \, d\omega . \end{aligned} \quad (3.26)$$

Finally, the expressions

$$\chi_1^{(0)} \pm \chi_2^{(0)} = R_\pm(\vec{q}, \omega) + iI_\pm(\vec{q}, \omega)$$

are put into Eq. (3.15) to compute the enhanced susceptibility. In the actual calculation, the steps from Eq. (3.21) on are carried out on a computer.

For the paramagnetic phase we can find the expression for the susceptibility function from Eq. (3.16) by putting $\bar{\Delta}(\nu) = 0$. This gives

$$a_l = -\pi N(0) \left(\frac{1}{ivQ + |\nu_l| + |\nu_l + \omega_n| + \Gamma} + \mathrm{c.c.} \right) \quad (3.27)$$

for $\nu_l(\nu_l + \omega_n) > 0$, and $a_l = 0$ otherwise. Similarly we have $b_l = c_l = d_l = 0$. The subsequent steps of the calculation are entirely parallel to those for the ordered phase.

It is interesting to examine the structure of the susceptibility function in the antiferromagnetic as well as the paramagnetic phase. One can easily show that, in the antiferromagnetic phase,

$$1 - V(\chi_1^{(0)} - \chi_2^{(0)}) = 0 \quad (3.28)$$

at $Q = 0$ and $\omega = 0$, and that this condition is equivalent to the gap equation [Eq. (2.17)]. For a small but finite Q, Eq. (3.28) can be satisfied by a small complex ω. In other words, the enhanced susceptibility has a complex pole, and this pole defines the spin-wave mode with wave vector Q. So the stability of the antiferromagnetic state and the elementary excitations of the system are both determined by the second term on the right-hand side of Eq. (3.15). Sokoloff[16] pointed out that, in absence of scattering, the first term has a pole at $Q = 0$ and $\omega = 2\Delta$. This is a Stoner-type mode directly across the energy gap. It will be shown in Sec. IV that this mode is very strongly damped, so that it is probably unobservable. In the paramagnetic phase we have $\chi_2^{(0)} = 0$, so the two terms become equal. The temperature at which the enhanced paramagnetic susceptibility diverges for $Q = 0$, $\omega = 0$ is the Néel temperature of the system.

IV. RESULTS OF NUMERICAL ANALYSIS

We have calculated the imaginary part of the enhanced susceptibility for the model defined in Sec. II in the antiferromagnetic phase at 300, 400, and 500 K, and in the paramagnetic phase at 530 and 600 K. The results are plotted in Figs. 6–10, where in the line-shape plots, the susceptibility function is normalized by the unenhanced static susceptibility χ_0 at $T = 0$. (χ_0 is a constant whose value depends on the material.) Aside from a boson distribution factor, the curves represent the inelastic neutron cross section for constant energy

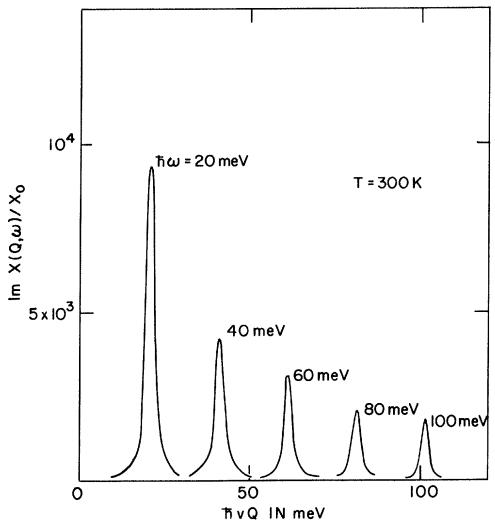

FIG. 6. Magnon line shapes at a low temperature.

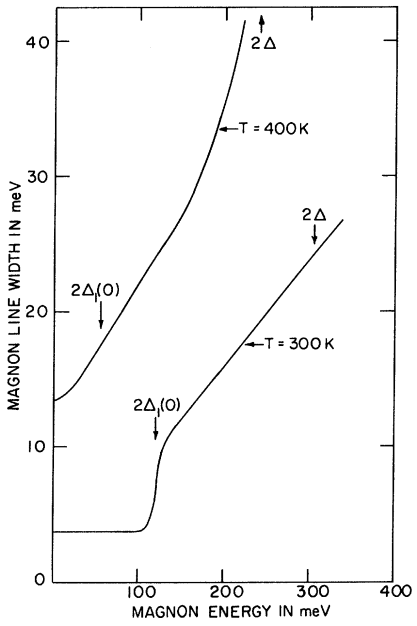

FIG. 8. Magnon linewidths as functions of energy and temperature.

scans with infinitely sharp resolution. As is clearly seen in Figs. 6 and 7, there are well-defined magnon peaks at $\omega \simeq vQ$ at 300 and 400 K. So the magnon velocity is very close to the band velocity, except that the temperature and scattering cause a downward shift of the order 5–10%. The magnon lines remain well defined until the magnon energy reaches the gap energy $2\Delta_1(0)$, and thereafter they broaden very rapidly as shown in Fig. 8. This is easy to understand because below the gap energy the magnons decay due to electronic viscosity, but above the gap energy they decay by electron-hole pair production. At 500 K, which is 15 K below the Néel temperature, the lines have a flat top centered around $Q = 0$, i.e., the magnetic reciprocal-lattice point (Fig. 9). In Fig. 10 we show the line shape at 530 K, 15 K above the Néel temperature. The lines are now peaked at $Q = 0$, and represent short-ranged short-lived excitations called paramagnons.[32,33] The lines at 600 K are very similar but much broader. Thus, the transition from magnons to paramagnons takes place gradually over a range

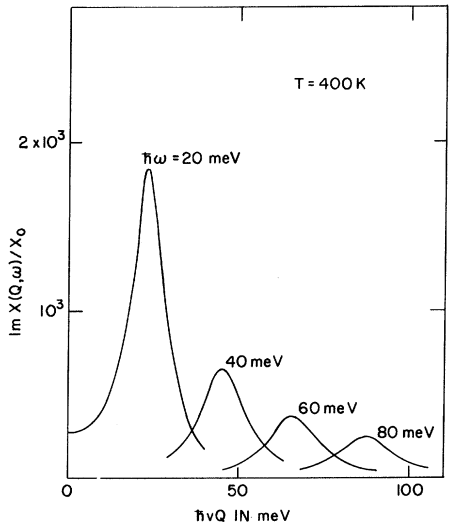

FIG. 7. Magnon line shapes at an intermediate temperature.

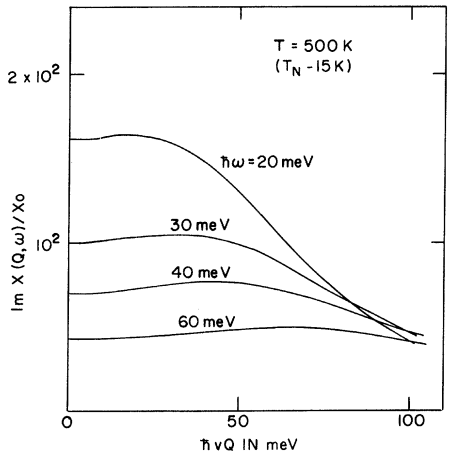

FIG. 9. Magnon line shapes just below the Néel temperature.

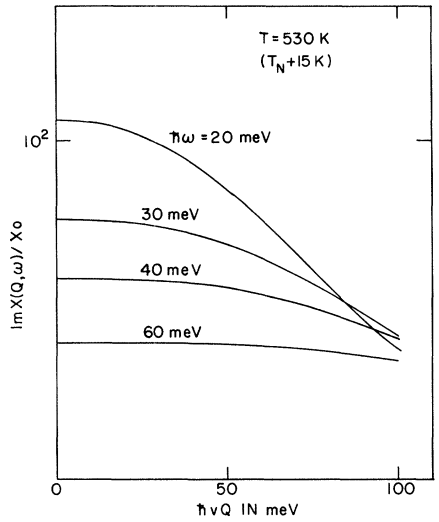

FIG. 10. Paramagnon line shapes just above the Néel temperature.

of temperature around T_N. For example, with realistic momentum resolution one can not experimentally detect the difference in line shapes at 500 and 530 K.

At low energies and temperatures the unenhanced susceptibility is well approximated by

$$\mathrm{Re}\chi^{(0)}(Q,\omega)=\mathrm{Re}\chi^{(0)}(0,0)-\alpha'^2(\omega^2-c^2Q^2)\ ,$$

$$\mathrm{Im}\chi^{(0)}(Q,\omega)=\gamma'\omega\ ,$$

where α', γ', and c are constants. It is more convenient to work with the quantity $V\chi^{(0)}(Q,\omega)$ because it is dimensionless. We define

$$\alpha=(\sqrt{V})\alpha'\ ,\quad \gamma=V\gamma'\ ;$$

then α and γ have the dimension of inverse energy. Thus, the enhanced susceptibility has the imaginary part

$$\mathrm{Im}\chi(Q,\omega)=\gamma\omega/\{V[\alpha^4(\omega^2-c^2Q^2)^2+\gamma^2\omega^2]\}\ . \quad (4.1)$$

It is found that the theoretical line shapes at 300 K for the model described in Sec. II can be closely fitted by $\alpha=2.13\times10^{-3}\,(\mathrm{meV})^{-1}$, $\gamma=1.36\times10^{-5}\,(\mathrm{meV})^{-1}$, and $c=0.96v$, with v as an adjustable parameter. This formula resembles very closely the result derived from the Heisenberg model except for the broadening.[34] The magnon linewidth at 300 K is $\gamma/\alpha^2=3$ meV. Since this value is very small compared to the instrumental resolution, it is a good approximation to treat the line shape as a δ function as we did in Ref. 19. Therefore, the intrinsic linewidth of the magnons does not affect our analysis of magnon velocity at room temperature.

The line shapes at 400 K can be fitted individually by Lorentzian functions, but the fitting parameters depend on the energy. The lines at 500 K cannot be fitted by any simple formula.

The present theory predicts that the damping rate of very long-wavelength magnons is finite. This conclusion is in disagreement with the predictions of the hydrodynamic theory of spin waves, which predicts a damping rate proportional to the square of the wave vector.[35] However, the hydrodynamic theory is developed for a uniform spin system where the magnon damping arises entirely from magnon-magnon interactions. The system considered in this paper is inherently nonuniform because of the impurity and phonon scatterings, and the magnon damping mechanism is also totally different. Therefore, there is no real conflict between the two theories.

Above T_N we find

$$\mathrm{Im}\chi(Q,\omega)=\frac{2(1-\epsilon)}{N(0)V^2}\,\frac{b\omega}{[\epsilon+a^2(\omega^2+v^2Q^2)]^2+b^2\omega^2}\ , \quad (4.2)$$

where $\epsilon=\ln(T/T_N)$, and a, b are functions of scattering and temperature.[19] At 530 K, we find $\epsilon=0.029$, $a=2.73\times10^{-3}\,(\mathrm{meV})^{-1}$, and $b=4.25\times10^{-3}\,(\mathrm{meV})^{-1}$, for the model of Sec. II.

For fixed neutron energy transfer ω, the integrated intensity of the neutron line is

$$I\propto(1-e^{-\beta\omega})^{-1}\int_{-\infty}^{\infty}\mathrm{Im}\chi(Q,\omega)\,dQ\ . \quad (4.3)$$

The integral can be estimated by using Eqs. (4.1) or (4.2). The result is

$$I\propto(1-e^{-\beta\omega})^{-1}\,\frac{\pi}{c\alpha}\,\mathrm{Re}\,\frac{1}{\sqrt{(\alpha^2\omega^2-i\gamma\omega)}} \quad (4.4)$$

for $T\ll T_N$, and

$$I\propto(1-e^{-\beta\omega})^{-1}\,\frac{2\pi(1-\epsilon)}{vaN(0)V}\,\mathrm{Im}\,\frac{1}{\sqrt{(\epsilon+a^2\omega^2-ib\omega)}} \quad (4.5)$$

for $T>T_N$. If we take the line for $\omega=20$ meV, we find

$$I(530\ \mathrm{K})/I(300\ \mathrm{K})=0.6\ .$$

This shows that when the temperature is increased from the antiferromagnetic region to the paramagnetic region, the neutron line merely broadens with very little loss of intensity.

For a fixed momentum transfer Q, the differential neutron cross section is given by

$$\frac{d\sigma}{d\Omega}\propto\int\frac{\mathrm{Im}\chi(Q,\omega)}{1-e^{-\beta\omega}}\,d\omega\ . \quad (4.6)$$

In the paramagnetic phase, the integration may be carried out for small Q with the result

$$\frac{d\sigma}{d\Omega}\propto\frac{K_BT}{\epsilon+a^2v^2Q^2}\ . \quad (4.7)$$

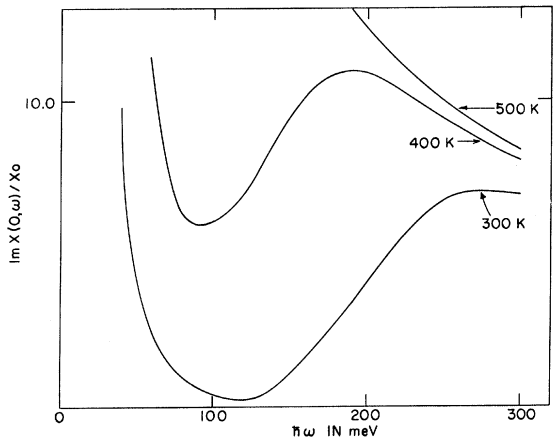

FIG. 11. Line shapes for the Stoner mode.

Since $\epsilon \cong (T - T_N)/T_N$, it follows that Eq. (4.7) is of the same form as that derived from the Heisenberg model in the quasistatic approximation.[30] However, the analogy with the Heisenberg model breaks down when one studies the dynamical effects. For example, Eq. (4.2) is totally different from the result of the spin-diffusion theory.[36] Therefore, the paramagnon mode is a different dynamical phenomenon from spin diffusion. It is also very easy to find the first and second moments of the neutron line in the paramagnetic phase:

$$\langle \omega \rangle = 0, \quad \langle \omega^2 \rangle = \epsilon/a^2 + v^2 Q^2,$$

where $\epsilon/a^2 \propto T - T_N$. For the Heisenberg model the first moment is nonvanishing, and there exists no second-moment formula in the vicinity of the critical temperature.

As was mentioned in Sec. III, there exists in itinerant electron antiferromagnets a Stoner-type mode, i.e., excitations directly across the energy gap. However, when the gap is broadened by scattering, this mode becomes strongly damped. We show in Fig. 11 the quantity $\mathrm{Im}\chi(Q, \omega)$ for ω near the gap energy at 300, 400, and 500 K. The curves diverge sharply at low energies as a result of the slightly diffused magnetic Bragg peak. The Stoner mode gives rise to a peak at $\omega = 280$ meV at 300 K, very close to $2\Delta_1(0) = 300$ meV. At 400 K, the Stoner peak is at 190 meV, which is closer to $2\Delta = 240$ meV than the gap energy $2\Delta_1(0) = 55$ meV. At 500 K, where the gap disappears altogether, the Stoner peak also disappears. However, a comparison of the vertical scale of Fig. 11 with those of Figs. 6, 7, and 9 makes it clear that the Stoner mode is too weak to be detectable by neutron diffraction.

In Sec. V, we will compare these calculated line shapes with the experimental results for CrMn alloys. The Fermi surfaces of these metals resemble two cubes, so they may nest into each other at a vertex after a translation along a (1, 0, 0) axis. The Fermi velocities of the two surfaces are along (1, 1, 1) directions. Thus, if a magnon is excited along (1, 0, 0), the band velocity that enters into the theory should be the component of the Fermi velocity in this direction, i.e., $v = v_F/\sqrt{3}$. That the magnon velocity is close to $v_F/\sqrt{3}$ also holds for the Fedders-Martin model.[11] In reality, the band velocity is further modified by mass enhancement effects due to electron-phonon and electron-magnon interactions. The latter interaction is discussed in Sec. V.

V. ELECTRON MASS ENHANCEMENT BY MAGNON AND PARAMAGNON INTERACTION

The electron mass enhancement due to electron-magnon and electron-paramagnon interactions in ferromagnetic systems has been discussed by many authors.[32,33,37–39] We will show here that this interaction also leads to a small mass shift in itinerant electron antiferromagnets. The self-energy diagram for the itinerant system is shown in Fig. 12. In mathematical terms we have

$$\tilde{\Sigma}(\vec{k}, \nu) = iV^2 \int [d^3q d\omega/(2\pi)^4] \chi(\vec{q}, \omega) \tilde{G}(\vec{k} - \vec{q}, \nu - \omega). \tag{5.1}$$

To obtain a first estimate of the effect, we calculate the integral under some simplifying approximations. We use the spherical Fedders-Martin model for the electron bands, and the spin-wave propagator

$$\chi(\vec{q}, \omega) = [4\Delta^2/N(0)V^2]/(\omega^2 - c^2q^2), \tag{5.2}$$

as found from the collisionless model. The electron propagator is, in real-frequency representation,

$$G(\vec{k}, \nu) = \frac{\epsilon_k + \nu}{\epsilon_k^2 + \Delta^2 - \nu^2}, \quad F(\vec{k}, \nu) = \frac{\Delta}{\epsilon_k^2 + \Delta^2 - \nu^2},$$

where ϵ_k is measured from the Fermi level. Substituting these into Eq. (5.1) and integrating over ω, we obtain

$$\Sigma_{11}(k, \nu) = \frac{\Delta^2}{N(0)} \int \frac{d^3q}{(2\pi)^3} \frac{1}{cq} \left[\left(1 + \frac{\epsilon_{k-q}}{E_{k-q}} \right) \frac{1}{\nu - E_{k-q} - cq} \right.$$

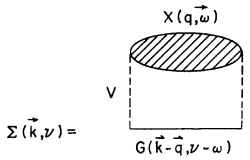

FIG. 12. Self-energy diagram due to paramagnon interactions.

$$+\left(1-\frac{\epsilon_{k-q}}{E_{k-q}}\right)\frac{1}{\nu+E_{k-q}+cq}\Bigg], \qquad (5.3)$$

where $E=(\epsilon^2+\Delta^2)^{1/2}$. We write this result as

$$\Sigma_{11}(k,\nu)=\frac{\Delta^2}{N(0)}\int d\epsilon\int d\epsilon'\frac{1}{\epsilon'}\Bigg[\left(1+\frac{\epsilon}{E}\right)\frac{1}{\nu-E-\epsilon'}+\left(1-\frac{\epsilon}{E}\right)\frac{1}{\nu+E+\epsilon'}\Bigg]F(\epsilon_k,\epsilon'),$$

where

$$F(\epsilon_k,\epsilon')=\int\frac{d^3q}{(2\pi)^3}\,\delta(\epsilon-\epsilon_{k-q})\,\delta(\epsilon'-cq).$$

For small q, we find

$$\epsilon_{k-q}\cong\epsilon_k-v_F q\cos\theta.$$

Then the integrations in F can be easily carried out. Thus,

$$F(\epsilon_k,\epsilon')=\frac{\epsilon'}{4\pi^2 v_F c^2}\,u\left[1-\left(\frac{\epsilon-\epsilon_k}{s\epsilon'}\right)^2\right],$$

where $s=v_F/c$, and $u(x)$ is the unit step function which vanishes for negative values of x. After integrating over ϵ' we find

$$\Sigma_{11}(k,\nu)=\frac{\Delta^2}{4\pi^2N(0)v_Fc^2}\int_{-2\Delta s}^{2\Delta s}d\epsilon\Bigg[\left(1+\frac{\epsilon}{E}\right)\ln\left|\frac{\nu-E-2\Delta}{\nu-E-|\epsilon-\epsilon_k|/s}\right|+\left(1-\frac{\epsilon}{E}\right)\ln\left|\frac{\nu+E-2\Delta}{\nu+E-|\epsilon-\epsilon_k|/s}\right|\Bigg], \qquad (5.4)$$

where we assume a spin-wave cutoff energy of 2Δ. Near the Fermi energy we may expand

$$\Sigma_{11}(k,\nu)=\Sigma_{11}(k_F,0)+\epsilon_k\left(\frac{\partial\Sigma_{11}}{\partial\epsilon_k}\right)+\nu\left(\frac{\partial\Sigma_{11}}{\partial\epsilon_k}\right)_0,$$

where the first term gives rise to a shift of the Fermi energy, and the other terms lead to a mass correction

$$m^*/m=\left[1+\left(\frac{\partial\Sigma_{11}}{\partial\nu}\right)_0\right]\Big/\left[1-\left(\frac{\partial\Sigma_{11}}{\partial\epsilon_k}\right)_0\right]. \qquad (5.5)$$

The derivatives are quite easy to evaluate. The results are

$$\left(\frac{\partial\Sigma_{11}}{\partial\nu}\right)_0=\frac{\Delta^2}{4\pi^2N(0)v_Fc^2}\left[\frac{2s}{s^2-1}\ln(4s^2-3)+\frac{4}{\sqrt{3}}\ln\left(\frac{2s+\sqrt{3}}{2s-\sqrt{3}}\right)\right],$$

$$\left(\frac{\partial\Sigma}{\partial\epsilon_k}\right)_0=-\frac{\Delta^2}{4\pi^2N(0)v_Fc^2}\,\frac{2}{s^2-1}\ln(4s^2-3). \qquad (5.6)$$

In the following, we estimate the size of the mass correction. The density of states of Cr is[40] 0.09 electrons/a.u. Ry $=30\times10^{33}$ electrons/erg cm^3. About half of these states will go into the condensed state, so the effective density of states per spin per band is $N(0)=4\times10^{33}$ per erg cm^3. We use the experimental values $\Delta=200$ meV, $c=1.3\times10^7$ cm/sec, and the calculated $v_F=5.1\times10^7$ cm/sec for paramagnetic Cr (with phonon enhancement included). Then we find $\Delta^2/4\pi^2N(0)v_Fc^2=0.07$ and $s=3.9$. These values lead to $m^*/m=1.2$, or that there is a 20% mass enhancement in the antiferromagnetic state. This would give a theoretical spin-wave velocity

$$c(\text{theory})=(v_F/\sqrt{3})(m/m^*)=2.5\times10^7\ \text{cm/sec},$$

which is almost a factor of 2 too high compared with the measured value. The discrepancy is probably due to subtle band effects not accounted for in this simple model.[41]

In the paramagnetic phase, we use Eq. (4.2) for χ. A similar calculation leads to

$$\frac{m^*}{m}=1+\frac{1-\epsilon}{4\pi^2N(0)v^3a^2}\ln\left(1+\frac{a^2v^2q_{\max}^2}{\epsilon}\right),$$

where $q_{\max}$ is the cutoff wave vector for paramagnons. It is reasonable to take $a^2v^2q_{\max}^2\cong\epsilon$. Together with $v=v_F/\sqrt{3}$, we find

$$m^*/m=1.14.$$

So the effective Fermi velocity which determines paramagnon line shape is

$$v_F(\text{theory})=v_F(m/m^*)=4.5\times10^7\ \text{cm/sec}.$$

This is in reasonable agreement with the measured value of 3.8×10^7 cm/sec.

ACKNOWLEDGMENTS

This work was stimulated by the experimental program of Dr. S. K. Sinha. The author wishes to thank him for his interest and encouragement during the investigation. It is also a great pleasure to thank Dr. J. B. Sokoloff and Dr. T. M. Rice for many informative discussions.

*Work performed in part in the Ames Laboratory of the U. S. Atomic Energy Commission, Contribution No. 2720.

[1]C. G. Shull and M. K. Wilkinson, Rev. Mod. Phys. 25, 100 (1953).

[2]G. Shirane and W. J. Takei, J. Phys. Soc. Japan 17, Suppl. B-111, 35 (1962).

[3]M. K. Wilkinson, E. O. Wollan, W. C. Koehler, and G. W. Cable, Phys. Rev. 127, 2080 (1962).

[4]P. J. Brown, C. Wilkinson, J. B. Forsythe, and R. Nathans, Proc. Phys. Soc. (London) 85, 1185 (1965).

[5]A. Arrott, S. A. Werner, and H. Kendrick, Phys. Rev. Letters 14, 1022 (1965).

[6]W. C. Koehler, R. M. Moon, A. L. Trego, and A. R. Mackintosh, Phys. Rev. 151, 405 (1966).

[7]A. L. Trego and A. R. Mackintosh, Phys. Rev. 166, 495 (1966).

[8]A. W. Overhauser, Phys. Rev. Letters 3, 414 (1959).

[9]A. W. Overhauser, Phys. Rev. 128, 1437 (1962).

[10]W. M. Lomer, Proc. Phys. Soc. (London) 80, 489 (1962).

[11]P. A. Fedders and P. C. Martin, Phys. Rev. 143, 245 (1966).

[12]A. Shibatani, K. Motizuki, and T. Nagamiya, Phys. Rev. 177, 984 (1969).

[13]J. C. Kimball and L. Falicov, Phys. Rev. Letters 20, 1164 (1968).

[14]S. H. Liu, Phys. Letters 27A, 493 (1968).

[15]T. M. Rice, A. S. Barker, Jr., G. I. Halperin, and D. B. McWhan, J. Appl. Phys. 40, 1337 (1969).

[16]J. B. Sokoloff, Phys. Rev. 185, 770 (1969); 185, 783 (1969).

[17]J. Zittartz, Phys. Rev. 164, 575 (1967).

[18]J. Als-Nielsen and O. W. Dietrich, Phys. Rev. Letters 22, 290 (1969).

[19]S. K. Sinha, S. H. Liu, L. D. Muhlestein, and N. Wakabayashi, Phys. Rev. Letters 23, 311 (1969).

[20]A. A. Abrikosov and L. P. Gor'kov, Zh. Eksperim. i Teor. Fiz. 39, 1781 (1960) [Soviet Phys. JETP 12, 1243 (1961)].

[21]S. Skalski, O. Betbeder-Matibet, and P. R. Weiss, Phys. Rev. 136, A1500 (1964).

[22]A. A. Abrikosov, L. P. Gor'kov, and I. E. Dzyaloshinski, *Methods of Quantum Field Theory in Statistical Physics* (Prentice-Hall, Englewood Cliffs, N. J., 1963), Chap. 7.

[23]V. Ambegaokar and L. Tewordt, Phys. Rev. 134, A805 (1964).

[24]V. Ambegaokar and A. Griffin, Phys. Rev. 137, A1151 (1965).

[25]V. Ambegaokar and J. Woo, Phys. Rev. 139, A1818 (1965).

[26]S. B. Nam, Phys. Rev. 156, 487 (1967).

[27]W. Shaw and J. C. Swihart, Phys. Rev. Letters 20, 1000 (1968).

[28]T. M. Rice (private communication).

[29]L. W. Bos, D. W. Lynch, and J. L. Stanford, Phys. Letters 30A, 17 (1969).

[30]L. van Hove, Physica 95, 1374 (1954).

[31]T. Izuyama, D. J. Kim, and R. Kubo, J. Phys. Soc. Japan 18, 1025 (1963).

[32]N. F. Berk and J. R. Schrieffer, Phys. Rev. Letters 17, 433 (1966).

[33]S. Doniach and S. Engelsberg, Phys. Rev. Letters 17, 750 (1966).

[34]R. J. Elliott and R. D. Lowde, Proc. Roy. Soc. (London) A230, 46 (1955).

[35]B. I. Halperin and P. C. Hohenberg, Phys. Rev. 188, 898 (1969).

[36]P.-G. de Gennes, in *Magnetism III*, edited by G. T. Rado and H. Suhl (Academic, New York, 1963), pp. 115–146.

[37]S. Nakajima, Progr. Theoret. Phys. (Kyoto) 38, 23 (1967).

[38]L. C. Davis and S. H. Liu, Phys. Rev. 163, 503 (1967).

[39]D. J. Kim, Phys. Rev. 167, 545 (1968).

[40]T. L. Loucks, Phys. Rev. 139, 223 (1965).

[41]R. P. Gupta and S. K. Sinha (unpublished).